Pergamon

Int. J. Heat Mass Transfer. Vol. 38, No. 17, pp. 3275–3284, 1995

0017-9310/95 $9.50+0.00

0017-9310(95)00021-6

Contact melting by a non-isothermal heating surface of arbitrary shape

S. A. FOMIN†, P. S. WEI
Institute of Mechanical Engineering, National Sun Yat-Sen University, Kaohsiung, Taiwan, China

and

V. A. CHUGUNOV
Department of Applied Mathematics, Kazan State University, Kazan, Russian Federation

(*Received* 5 *April* 1994 *and in final form* 27 *December* 1994)

Abstract—Contact melting a material by a moving heater of arbitrary shapes with non-isothermal working surface is systematically investigated. A pressure exerted by the heater continuously squeezes the molten layer out of the close-contact region. The melting material has non-linear physical properties including temperature dependent conductivity, viscosity and non-Newtonian behaviors. By using a scale analysis momentum and energy equations are simplified. An iterative numerical procedure based on a boundary elements method is developed. Computed results show a good agreement with the analytical solutions that are available for a parabolic isothermal heating surface and constant physical properties. Influences of temperature distributions along the working surface and lengths of the heater on the thickness of the molten layer are found. A comparison between these factors is made. An appropriate distribution of the heat source within the heater is also proposed.

1. INTRODUCTION

Melting a solid by a close contact with a heating surface takes place in numerous natural and technological processes. Two types of applications can be categorized [1]. In one group the material lies on the heating surface and is pressed against it by some external force such as the weight of melting material. This situation occurs when the unfixed phase-change material melts in an enclosure. The other group of applications involves a moving heater melting its way through the surrounding solid. This phenomena arises in such fields as geology, nuclear technology, welding, oil industry and thermal drilling of rocks and glaciers.

Thermal drilling is commonly recognized as the most effective method to bore glaciers [2, 3]. Drilling rocks and soils by a thermopenetrator [4, 5] is a relatively new method in mining engineering. It has advantages over a traditional rotary drilling. For example, rock fracturing, debris removal and wall stabilization are accomplished in a single integrated operation.

Theories of contact melting have been developed since the last decade. Melting inside the capsules for energy storage was investigated by Moore and Bayazitoglu [6], Roy and Sengupta [7] and Saito *et al.* [8]. Bejan [9], and Tyvand and Bejan [10] studied contact melting induced by friction. They accounted for melting ice due to a decrease in the melting point by applying an external load. Enhancement of heat transfer and reduction of thermal resistance in the molten layer by machining slots on the heating surface were analytically, numerically and experimentally investigated by Saito *et al.* [11]. Contact melting under rotation conditions was studied by Taghavi [12]. Moallemi and Viskanta [1, 13] used a marching-integration procedure to obtain complete numerical results of contact melting for a moving horizontal cylindrical heater. Measured surface temperatures of the heater and melting velocities under rectangular and circular cylinder-shaped heater are provided by Webb *et al.* [14].

Although previous investigations highlight the main characteristics of contact melting, the effects of temperature-dependent properties were ignored. Heat conduction to the surrounding solid was also neglected. This is only valid when the latent heat is greater than the sensible heat in solid. Heat conduction in the heater was not investigated. The influence of the shape of heating surface and temperature distribution on it was not analysed. Although Fomin and Wei [15] accounted for shape factor and temperature dependent properties, the heating surface was assumed to be isothermal.

In the present study a general mathematical model of contact melting of a material with temperature-dependent physical properties is developed. The molten material is considered to be a non-Newtonian liquid of the Ostvald-de-Waele type, which was experimentally confirmed for a molten rock or magma [16].

†On leave from: Department of Applied Mathematics, Kazan State University, Kazan 42008, Russian Federation.

NOMENCLATURE

B Newtonian viscosity $= \exp(E/RT_1)$
B_0 scale for B
C_c solid-to-liquid specific heat ratio $= c_s/c_l$
C_h transverse-to-tangential length scale ratio in molten layer $= h_0/l$
c_l liquid specific heat
c_s solid specific heat
E activation energy
h dimensionless molten layer thickness $= \tilde{h}/h_0$
h_0 characteristic thickness of molten layer
j heat source distribution function
J function defined by equation (27)
k conductivity
k_l dimensionless liquid conductivity $= \tilde{k}_l/k_0$
k_0 characteristic conductivity of liquid
K_0 modified Bessel's function of the second kind and zeroth order
k_s dimensionless solid conductivity $= \tilde{k}_{s0}/k_0$
k_{s0} characteristic conductivity of solid
l longitudinal characteristic length
L latent heat for melting
M, M_i points on boundary and interior region Ω
n flow index describing non-Newtonian fluid or direction normal to the surface
p liquid pressure
Pe modified solid Peclet number $= Vl/\alpha_s$
Pe_l modified liquid Peclet number $= V\rho_s l/(\alpha_l \rho_l)$
q heat flux conducted to solid at melting surface
q_w heat flux on the working surface
r polar coordinate
$\mathbf{r}$ position vector
R gas constant
Re modified Reynolds number $= \rho_s Vl/\mu_0$
Ste Stefan number $= L/[c_l(T_m - T_\infty)]$
T temperature
T_{w0} characteristic surface temperature of the heater $= T_m - (T_m - T_\infty) C_h Pe_l(Ste + C_c)$
T_∞ ambient temperature
V dimensional melting speed
v_0 characteristic tangential velocity $= Vl\rho_s/(h_0\rho_l)$
v_ξ dimensionless tangential velocity $= \tilde{v}_\zeta/v_0$
v_η dimensionless transverse velocity $= \tilde{v}_\eta \rho_l/(\rho_s v)$
w external load pressure
x $\tilde{x}/l$, as shown in Fig. 1
x_* location of the stagnation point
z $\tilde{z}/l$, as shown in Fig. 1.

Greek symbols
α_l liquid diffusivity $= k_0/(c_l\rho_l)$
α_s solid diffusivity $= k_{s0}/(c_s\rho_s)$
α_1, α_2 functions determined in equation (13)
Γ generating line, as illustrated in Fig. 1
$\Delta(x)$ Dirac delta function
ζ tangential coordinate $= \tilde{\zeta}/l$, as shown in Fig. 1
ζ_* tangential location where $\partial p/\partial\xi = 0$
η transverse coordinate $= \tilde{\eta}/\tilde{h}$, as shown in Fig. 1
η_0 transverse coordinate where $\partial v_\zeta/\partial\eta = 0$
θ dimensionless solid temperature $= (T - T_\infty)/(T_m - T_\infty)$
$\tilde{\Theta}$ Kirchhoff transformation of solid temperature
θ_l dimensionless liquid temperature $= (T_l - T_m)/(T_{w0} - T_m)$
μ dimensionless dynamic viscosity $= \tilde{\mu}/\mu_0$
μ_0 scale for viscosity $= B_0(Pe_l/B_0)^{\frac{2(n-1)}{2n+1}}(V\rho_s/l\rho_l)^{\frac{n-1}{2n+1}}$
ρ density
Σ surface, as illustrated in Fig. 1
Ω domain of solid, as illustrated in Fig. 1
Ω_h domain of heater.

Superscripts
~ dimensional quantity.

Subscripts
h heater
l liquid
m melting
s solid
w working surface
1, 2 end points, as illustrated in Fig. 1.

The heating surface of an arbitrary shape is non-isothermal. It has a hole in the center for some applications [2–5]. The appropriate heat sources within the heater are proposed.

2. SYSTEM MODEL AND ANALYSIS

A schematic sketch of a contact melting induced by a heater moving at a constant speed V is illustrated in

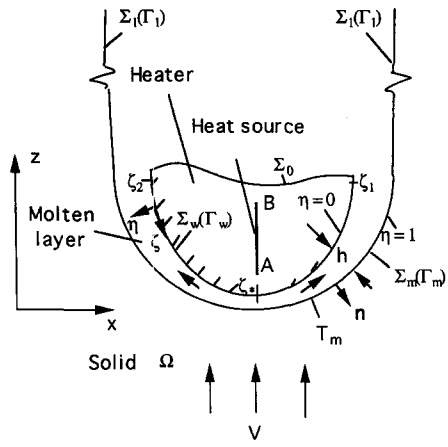

Fig. 1. Schematic sketch of the model and coordinate system.

Fig. 1. The solid occupies a semi-infinite domain Ω. Boundaries of solid consists of a surface Σ_m, where the phase change occurs, and a surface Σ_l determined by different melting techniques. The surface of the heater can be either an axisymmetric surface Σ_w generated by a curve Γ_w or a cylindrical surface Σ_w having a boundary curve Γ_w. The axisymmetric (r, z) or Cartesian (x, y, z) coordinate systems, therefore, are attached to the moving heater. The z coordinate directs upwards, with the solid moving in the positive z-direction. Since the length in the y-direction is considered sufficiently larger than those in x- and z-directions, respectively, the model becomes a two-dimensional case in coordinates (x, z). A local two-dimensional curvilinear orthogonal coordinate system (ζ, η), which is often used in the boundary layer problem, is applied. The coordinates $\eta = 0$, 1 are fixed on the working surface of the heater and the melting surface, respectively. The primary assumptions made are the following :

(1) The melting rate or migrating speed V is constant relative to the heater. This is confirmed by Moallemi and Viskanta [1] by measuring migrating velocities in melting solid n-octadecane.

(2) A relatively thin molten layer [1] and high melting velocities ($Pe \gg 1$) are treated due to a high force exerted and heat transferred from the heat source.

(3) Viscosity, and thermal conductivities in solid and liquid are functions of temperature. The molten thin layer can be a non-Newtonian fluid [16].

2.1. *Governing equations in the molten layer*

Governing equations are expressed in curvilinear coordinates (ζ, η) which are related to Cartesian coordinates (x, z) by (see Fig. 1)

$$x = x_h(\zeta) + hC_h\eta\frac{dz_h}{d\zeta} \quad z = z_h(\zeta) - hC_h\eta\frac{dx_h}{d\zeta} \tag{1}$$

where the tangential and transverse length scales of the molten layer are chosen to be a typical size of the heater l and thickness of the thin layer h_0, respectively. The scale for tangential velocity is $v_0 = Vl\rho_s/\rho_l h_0$ that is determined by a mass balance in the molten material, while the scale for the transverse velocity in the melt is $V\rho_s/\rho_l$. The fluid layer is driven by the pressure gradient, which is of the same magnitude as the viscous force. This leads to $h_0 = [Vl^2\mu_0\rho_s/(\rho_l w)]^{1/3}$, where the characteristic viscosity is $\mu_0 = B_0(v_0/h_0)^{n-1}$. As a consequence, the ratio of the characteristic thickness of the molten layer to the tangential length scale $C_h = h_0/l = (B_0/w)^{1/(2n+1)}(V\rho_s/l\rho_l)^{n/(2n+1)}$. As it was justified theoretically and by the experiment [1, 3, 4, 14] for contact melting of different materials parameters Re, $C_h \ll 1$. The continuity and momentum equations after neglecting the terms of $O(Re)$, $O(C_h)$ reduce to

$$\frac{1}{x_h^v}\frac{\partial}{\partial\eta}(hx_h^v v_\zeta) + \frac{\partial v_\eta}{\partial\eta} = 0 \tag{2}$$

$$\frac{dp}{d\zeta} = \frac{1}{h}\frac{\partial}{\partial\eta}\left[\frac{B(\theta_l)}{h}\left|\frac{1}{h}\frac{\partial v_\zeta}{\partial\eta}\right|^{(n-1)}\frac{\partial v_\zeta}{\partial\eta}\right] \tag{3}$$

where power $v = 1$ for axisymmetric heating surface and $v = 0$ when the heating surface is two-dimensional in Cartesian coordinates (x, z). The associate boundary conditions of an accuracy of $O(C_h)$ are

$$v_\zeta = 0 \quad v_\eta = 0 \quad \text{at}\,\eta = 0 \tag{4}$$

$$v_\zeta = 0 \quad v_\eta = -\frac{dx_h}{d\zeta} \quad \text{at}\,\eta = 1. \tag{5}$$

Pressures at the exit points of the molten layer are denoted by $p(\zeta_1) = p_1$ and $p(\zeta_2) = p_2$, respectively. The force balance between the load exerted by the heater on the thin layer and stresses in the molten layer with an accuracy of $O(C_h)$ is governed by

$$\frac{1}{|\Sigma_h|}\int_{\Sigma_h} p\frac{dx_h}{d\zeta}d\Sigma = 1. \tag{6}$$

The ratio of heat generation due to viscous stresses to conduction is generally very small and is around 10^{-4}–10^{-3} for contact melting with a high-energy load. Hence the energy equation reduces to

$$c_l Pe_l C_h\left(v_\zeta\frac{\partial\theta_l}{\partial\zeta} + \frac{v_\eta}{h}\frac{\partial\theta_l}{\partial\eta}\right) = \frac{1}{h}\frac{\partial}{\partial\eta}\left(\frac{k_l}{h}\frac{\partial\theta_l}{\partial\eta}\right) \tag{7}$$

where temperature is scaled by $(T_{w0} - T_m) = (T_m - T_\infty)C_h Pe_l(Ste + C_c)$. The associate boundary conditions are

$$\theta_l = \theta_* f(\zeta) \quad \text{at}\,\eta = 0 \quad \theta_l = 0 \quad \text{at}\,\eta = 1 \tag{8}$$

where $f(\zeta)$ determines the temperature distribution on the working surface of the heater. The Stefan boundary condition representing an energy balance at the melting surface with an accuracy of $O(C_h)$ yields

$$-k_l\frac{\partial\theta_l}{\partial\eta} = \frac{1}{Ste + C_c}\left(Ste\,h\frac{dx_h}{d\zeta} + C_c qh\right) \tag{9}$$

where the scale for heat flux is $q_0 = k_{s0}(T_m - T_\infty)Pe/l$

as it can be estimated from the energy equation in solid. In equation (7) a condition for a vanished v_ζ at the stagnation point $\zeta = \zeta_*$ is used.

2.2. *Determination of conduction to solid*

In order to calculate heat conduction to solid, a solution of the energy equation in solid is needed. The energy equation is

$$\nabla^2\bar{\theta} - Pe\frac{\partial\bar{\theta}}{\partial z} = Pe\left(\frac{c_s}{k_s} - 1\right)\frac{\partial\bar{\theta}}{\partial z} \tag{10}$$

where the dimensionless temperature is defined by the Kirchhoff transformation as

$$\bar{\theta} = \int_0^{\theta} k_s\,\mathrm{d}\theta \Big/ \int_0^1 k\,\mathrm{d}\theta$$

[17]. An introduction of this dependent variable can avoid certain difficulties associated with the temperature-dependent conductivity k_s. Boundary conditions are

$$\bar{\Theta} = 1 \quad \text{on}\,\Sigma_m\,; \quad \bar{\theta} = \bar{\theta}_1 \quad \text{on}\,\Sigma_1 \tag{11}$$

Solid temperature far from the working surface $\bar{\Theta} \to 0$ as $R \to \infty$.

A solution of equation (10) in an integral form can be presented as

$$\begin{aligned}\bar{\Theta}(M_i) = {} & \int_{\Gamma_m+\Gamma_1} -\frac{\partial\bar{\Theta}}{\partial n}\phi\,\mathrm{e}^{\frac{Pe}{2}(z_i-z)}\,\mathrm{d}\Gamma \\ & + \int_{\Gamma_1}(\bar{\Theta}_1 - 1)\left[\mathrm{e}^{\frac{Pe}{2}(z_i-z)}\frac{\partial\phi}{\partial n}\right. \\ & \left. - \phi\frac{\partial}{\partial n}(\mathrm{e}^{\frac{Pe}{2}(z_i-z)})\right]\mathrm{d}\Gamma \\ & - Pe\int_\Omega \phi\,\mathrm{e}^{\frac{Pe}{2}(z_i-z)}\left(\frac{c_s}{k_s} - 1\right)\frac{\partial\bar{\Theta}}{\partial z}\,\mathrm{d}\Omega \quad M_i \in \Omega\end{aligned} \tag{12}$$

where the right-hand side is a sum of single- and double-layer potentials.

For 2D and axisymmetric cases the surface integrals over surfaces Σ_m, Σ_1 in equation (12) are replaced by line integrals along their generating curves, Γ_m and Γ_1, respectively. The fundamental solution ϕ satisfies the equation $\nabla^2\phi - (Pe/2)^2\phi = 0$. In a 2D case, the fundamental solution is $\phi(M, M_i) = K_0\{[(x-x_0)^2 + (z-z_0)^2]^{1/2}Pe/2\}/2\pi$. For an axisymmetric surface the fundamental solution in cylindrical coordinates can be obtained from a 3D model as proposed in [18] for the Laplace equation. In our case the fundamental solution yields

$$\phi = \frac{r}{\pi}\int_{\alpha_1}^{\alpha_2} \exp\left(-\frac{Pe\,t}{2}\right)[(\alpha_2^2 - t^2)(t^2 - \alpha_1^2)]^{-1/2}\,\mathrm{d}t \tag{13}$$

where $\alpha_1 = [(r-r_i)^2 + (z-z_i)^2]^{1/2}$ and $\alpha_2 = [(r+r_i)^2 + (z-z_i)^2]^{1/2}$.

Based on a potential theory, equation (12) by taking a one-side limit from an interior point in solid to the boundary $\Gamma_1 + \Gamma_m$ leads to

$$\begin{aligned}& \int_{\Gamma_m+\Gamma_1}\left(-\frac{\partial\bar{\Theta}}{\partial n}\right)\phi\,\mathrm{e}^{\frac{Pe}{2}(z_i-z)}\,\mathrm{d}\Gamma \\ & = \int_{\Gamma_1}(1-\bar{\Theta}_1)\left[\mathrm{e}^{\frac{Pe}{2}(z_i-z)}\frac{\partial\phi}{\partial n} - \phi\frac{\partial}{\partial n}(\mathrm{e}^{\frac{Pe}{2}(z_i-z)})\right]\mathrm{d}\Gamma \\ & \quad + Pe\int_\Omega \phi\,\mathrm{e}^{\frac{Pe}{2}(z_i-z)}\left(\frac{c_s}{k_s} - 1\right)\frac{\partial\bar{\Theta}}{\partial z}\,\mathrm{d}\Omega \\ & \quad + \begin{cases} 1 & M_i \text{ on } \Gamma_m \\ \dfrac{1+\bar{\Theta}_1}{2} & M_i \text{ on } \Gamma_1\,. \end{cases}\end{aligned} \tag{14}$$

Equations (12) and (14) provide a general description of temperature fields in bulk solid and heat flux at the melting surface, respectively. It reveals that temperature and heat flux on surface Σ_m are not affected by thermal conditions on surface Σ_1 if the Peclet number $Pe \gg 1$. In this case, the surface integrals over Γ_1 in equations (12) and (14) can be ignored. The heat flux across the melting surface can be represented as

$$q = -\frac{1}{Pe}\left[\frac{\partial\Theta}{\partial n}\right]_{\Gamma_m}\int_0^1 k_s\,\mathrm{d}\Theta. \tag{15}$$

When the shape of the melting surface is known equations (12) and (14) are solved numerically by iterations. It should be noted that, although the domain Ω is semi-infinite, temperature perturbations are concentrated in the thermal boundary layer, whose thickness is of $O(1/Pe)$. Discretization of Ω, therefore, does not bring difficulty.

2.3. *Heat conduction in the heater*

The heat conduction equation in the heater and associated boundary conditions on its working surface yield

$$\nabla^2\Theta_h = j \tag{16}$$

$$\Theta_h|_{\Sigma_w} = k_h C_h \Theta_1|_{\eta=0} \tag{17}$$

$$\left.\frac{\partial\Theta_h}{\partial n}\right|_{\Sigma_m} = \left.\left(\frac{k_1}{h}\frac{\partial\Theta_1}{\partial\eta}\right)\right|_{\eta=0}. \tag{18}$$

On the boundary Σ_0 which is not in contact with the molten material (Fig. 1) the insulation condition is assumed in order to avoid energy dissipation. That is

$$\left.\frac{\partial\Theta_h}{\partial n}\right|_{\Sigma_0} = 0. \tag{19}$$

In equations (16)–(18) the scales for the heat source energy j and temperature θ_h of the heater are chosen as $j_0 = k_0(T_{w0} - T_m)/(l^2 C_h)$ and $T_{h0} = j_0 l^2/k_h$ since heat fluxes on the left and right hand sides of the equation (18) should be of the same order. With the accuracy of $O(K_h C_h)$ boundary condition (17) can be substituted by $\theta_h = 0$. The latter provides a separation of

the heat conduction problem in the heater from the heat and mass transfer processes in the molten layer.

A solution of the equation (16) by substituting boundary conditions (17)–(19) yields [18]

$$\Theta_h(M_i) = \int_{\Sigma_w} \left(-\frac{\partial \Theta_h}{\partial n}\right)\phi(M, M_i)\,d\Sigma + \int_{\Sigma_w+\Sigma_0} \Theta_h \frac{\partial \phi}{\partial n} d\Sigma - \int_{\Omega_h} \phi(M, M_i) j(M)\,d\Omega, \quad M_i \in \Omega_h \quad (20)$$

where fundamental solutions of Laplace equation in 2D and 3D cases are $\phi(M, M_i) = (1/2\pi)\ln(1/r)$, $\phi(M, M_i) = (1/4\pi)(1/r)$, respectively. In an axisymmetric case $\phi(M, M_i) = (r/\pi)K(1-\alpha_1^2/\alpha_2^2)/\alpha_2$, where K is a complete elliptic integral of the first kind. Taking point M_i to the boundary and accounting for the jump of the second integral on the right hand side of equation (20) yields a boundary integral equation

$$\int_{\Sigma_w} \left(-\frac{\partial \Theta_h}{\partial n}\right)\phi(M, M_i)\,d\Theta + \int_{\Sigma_m+\Sigma_0} \Theta_h \frac{\partial \phi}{\partial n} d\Sigma = \int_{\Omega} \phi(M, M_i) j\,d\Omega + \Theta_h(M_i)/2. \quad (21)$$

When the heat source function j in equation (21) is known the heat flux on the working surface can be calculated from equation (21). This problem can also be treated as inverse problem where j is an unknown function and the heat flux on the working surface is calculated from the solution of heat transfer problem in the molten layer. It can be assumed that the heat source is concentrated on the segment AB of the straight line $x = x_*$ (Fig. 1) and j is approximated by a linear function :

$$j(x, z) = \begin{cases} \left[C\left(z - \frac{B+A}{2}\right) + \frac{1}{B-A}\right]\Delta(x - x_*) & \text{if } z \in [A, B] \\ 0 & \text{if } z \notin [A, B] \end{cases} \quad (22)$$

where the unknown parameter C satisfies an inequality $0 \leqslant C \leqslant 2/(B^2 - A^2)$. The function j is chosen to satisfy the conditions : (a) $j > 0$ since only source exists in the heater; and (b) $\int_{\Omega_h} j\,d\Omega = 1$ that indicates a constant total capacity of the source.

The inverse problem is formulated as a problem of minimizing the functional

$$\min_C \phi(C) = \int_{\Sigma_w} \left[q_w(C) - \left(\frac{k_l}{h}\frac{\partial \Theta_l}{\partial \eta}\right)_{\eta=0}\right]^2 d\Sigma. \quad (23)$$

It can be shown that the inverse problem for the convex uniform functional (23) on the chosen set of variables C has the unique solution [19].

3. METHOD OF SOLUTION

3.1. *Distributions of velocity and pressure in molten layer*

Integrating equation (3) twice yields

$$v_\zeta = \operatorname{sign}\left(-\frac{dp}{d\zeta}\right)\left|\frac{dp}{d\zeta}\right|^{\frac{1}{n}} h^{\frac{1+n}{n}} \int_0^\eta \times \operatorname{sign}(\eta_0 - \eta)\left|\frac{\eta_0 - \eta}{B(\Theta_l)}\right|^{\frac{1}{n}} d\eta \quad (24)$$

where the first relation in equation (4) and a condition indicating the maximum velocity (i.e. $\partial v_\zeta/\partial \eta = 0$) at $\eta = \eta_0$ are used. The velocity gradient $\partial v_\zeta/\partial \eta > 0$ for $\eta < \eta_0$, while $\partial v_\zeta/\partial \eta < 0$ for $\eta > \eta_0$. A longitudinal coordinate ζ_* exists between ζ_1 and ζ_2 such that $dp/d\zeta < 0$ for $\zeta_* < \zeta < \zeta_1$ and $dp/d\zeta > 0$ for $\zeta_2 < \zeta < \zeta_*$. Introducing the first relation in equations (5) into equation (24) the location of η_0 is determined

$$\int_0^1 \operatorname{sign}(\eta_0 - \eta)\left|\frac{\eta_0 - \eta}{B(\Theta_l)}\right|^{\frac{1}{n}} d\eta = 0. \quad (25)$$

Substituting equation (24) into the continuity equation (2), integrating with respect to η, and introducing the second relation in equations (4) leads to

$$v_\eta = \operatorname{sign}\left(\frac{dp}{d\zeta}\right)\frac{1}{x_h^\nu}\frac{\partial}{\partial \zeta}\left[h^{\frac{1+2n}{n}} x_h^\nu \left|\frac{dp}{d\zeta}\right|^{\frac{1}{n}} J(\eta, \zeta)\right] \quad (26)$$

where the function J yields

$$J(\eta, \zeta) = \int_0^\eta (\eta - \zeta)\operatorname{sign}(\eta_0 - \zeta)\left|\frac{\eta_0 - \zeta}{B(\Theta_l)}\right|^{\frac{1}{n}} d\zeta. \quad (27)$$

Integrating the second relation in equations (5) with respect to ζ, substituting equations (26), and using the condition $dp/d\zeta = 0$ at $x_* = x(\zeta_*)$ leads to

$$p = -\int_{\zeta_2}^{\zeta} \frac{\operatorname{sign}[x_h(\zeta) - x_*]|x_h^{\nu+1}(\zeta) - x_*^{\nu+1}|^n}{(\nu+1)^n [x_h^\nu J(1, \zeta)]^n h^{2n+1}} d\zeta + p_2 \quad \zeta_2 < \zeta < \zeta_1 \quad (28)$$

were the critical location ζ_* can be determined by substituting the boundary condition $p = p_1$ at $\zeta = \zeta_1$ into equation (28). This gives

$$\int_{\zeta_2}^{\zeta_1} \frac{\operatorname{sign}[x_h(\zeta) - x_*]|x_h^{\nu+1}(\zeta) - x_*^{\nu+1}|^n}{(\nu+1)^n [x_h^\nu J(1, \zeta)]^n h^{2n+1}} d\zeta = p_2 - p_1. \quad (29)$$

3.2. *Solution procedure*

The solution procedure is described as follows.

(1) An approximate linear initial temperature θ_l satisfied by $\theta_w = f(\zeta)$, $\theta_* = 1$ at the working surface is assumed. The Peclet number and shape of the working surface of the heater are specified.

(2) The location η_0 is obtained from equation (25).

(3) Heat flux distribution on the melting surface is calculated from equations (14) and (15).

(4) Thickness of the molten layer is obtained from equation (9).

(5) The critical tangential location x_* is determined from equation (29).

(6) Transverse and tangential velocities, and pressure are calculated from equations (26), (24) and (28), respectively.

(7) The constant θ_* is obtained by substituting equation (28) into equation (6).

(8) An improved temperature profile of liquid is obtained by solving energy equation (7) subject to boundary conditions (8) and melting temperature at the melting surface.

(9) Steps 2–8 are repeated until temperature profiles in the molten layer converge.

(10) The parameter C in the function j is found from the solution of the inverse problem governed by equations (21) and (23).

4. RESULTS AND DISCUSSION

Among the numerous applications the contact melting of rock and ice are of great interest. Physical properties of these materials are well documented and, for example, can be found in [3, 4]. Temperature-dependent conductivity k_l and Newtonian viscosity B can be represented by the equations $k_l = 1+e\theta_l^d$ and $B = \exp(E/RT_l)$, respectively. For a molten rock they are approximately [4] : $k_l = 1+2.4\theta_l^{1.46}$ and $B = \exp(30036/T_l)$. Flow indexes $n = 0.8$ and 1 are referred to the molten rock [16] and water, respectively. Even though numerical computations provided below are for rock and ice melting conditions, general conclusions can be drawn.

4.1. *Heat conduction in the surrounding solid*

Since the molten layer is very thin the shape of the melting surface is similar to that of the working surface. That is to say, the melting surface Σ_m equal to Σ_w with an accuracy of $O(C_h)$. Integrals over the generating curve of the melting surface in the equations (12), (14), therefore, can be substituted by the integrals along the contour Γ_w. As a result, heat conduction in the solid can be studied separately from heat transfer across the molten region.

Heat flux distributions on the melting surface are presented in Fig. 2. Heat flux on an elliptical melting surface Fig. 2(a) are found to be in agreement with those obtained in [20] for a welding pool of an elliptical shape. For the parabolic melting surface computed results coinside with analytical close-form solution obtained in [21] by introducing parabolic coordinates. This confirms the accuracy of the boundary elements method used in present study. Solid and dashed lines in Fig. 2(b) represent heat flux distributions on a toroidal melting surface that were

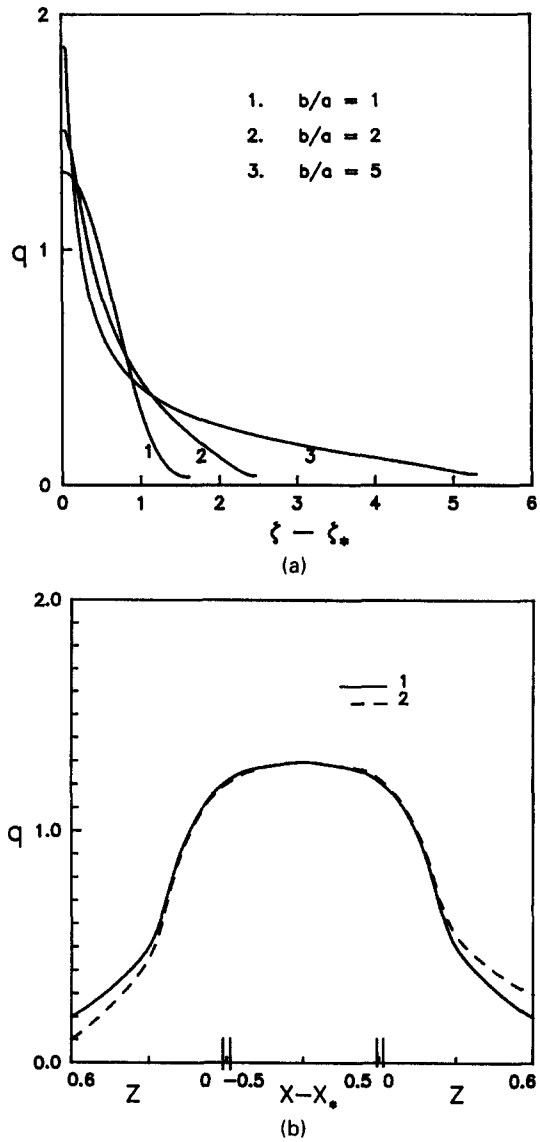

Fig. 2. Heat fluxes along a melting surface of an elliptical shape : (a) generated by equation $(x-x_*)^2/a^2+z^2/b^2 = 1$ and (b) along the melting surface generated by the circular curve with vertical parts for $Pe = 5$. Solid line, solution of equation (14) for ϕ determined by modified Bessel function K_0 ; dashed line, solution of equation (14) for ϕ defined by equation (13).

obtained when the fundamental solution ϕ in equation (14) was determined by the modified Bessel function K_0 and by equation (13), respectively. The generating curve of the melting surface is a half of the circle $\{(x-x_*)^2+z^2 = 0.25\ ;\ z < 0\}$ with vertical straight line segments $\{x = x_*-0.5\ ;\ x = x_*+0.5;\ 0 \leqslant z \leqslant z_0\}$. It can be seen that heat fluxes differ slightly only in vicinity of the ends of generating curve. For different shapes of heaters and Peclet numbers $Pe > 1$ numerical computations exhibit similar results. Therefore, the effect of axisymmetry is insignificant for toroidal surfaces and Peclet numbers

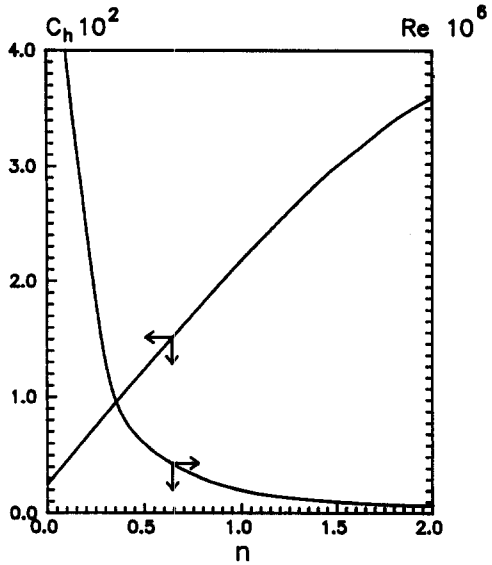

Fig. 3. The parameter C_h and Reynolds number as a function of flow index.

$Pe > 1$. As a result, a fundamental solution for a 2D flat model can be used for computations of heat flux and temperature in surrounding solid.

4.2. *Heat transfer in the molten layer*

The ratio between the characteristic thickness of the molten layer and dimension of the heater is $C_h = (B_0/w)^{1/(1+2n)}[V\rho_s/(l\rho_l)]^{n/(2n+1)}$. The thickness of the molten layer therefore is decreased by reducing the viscosity, melting rate, density of solid, longitudinal location, and increasing the external force, and liquid density, respectively. Furthermore, a decrease in the flow index, n, reduces the thickness or parameter C_h, as shown in Fig. 3. The reason for this is that a decrease in the flow index reduces the viscosity and increases the velocity gradient near the wall. As a consequence, the thickness of the molten layer decreases and tangential velocity increases. The Reynolds number subsequently increases. The computed results show that the parameter C_h and Reynolds number for melting rock can be of the order of 10^{-1}–10^{-2} and 10^{-6}, respectively, for melting rock conditions.

If working surface of the heater is isothermal and parabolic in shape, and the melt is Newtonian liquid with constant physical properties then simple analytical solutions in closed form can be obtained [21]. Numerical results and simplified analytical solutions for distributions of temperature and heat flux, pressure, and thickness of the molten layer by using a mean and temperature dependent viscosities are presented in Fig. 4. The molten layer is assumed to be a Newtonian fluid having a constant specific heat and conductivity. It can be seen that agreement between the numerical and analytical results is very good.

In order to investigate the influence of temperature distribution θ_w along the working surface Σ_w, a series of computations for different variations of temperature were carried out. Temperature on Σ_w was specified by the equation $\theta_w^1 = \theta_* + 4\Delta\theta x^2$ where $\Delta\theta$ is temperature difference along Σ_w between the stagnation point $\zeta = \zeta_* = 0$ and end point ζ_1 of the working surface. The heater is axisymmetric, without a hole in the center generated by curve Γ_w which is determined by the equation $z = 10(x^2 - 0.25)$ and $0 \leqslant x \leqslant 0.5$. The dimensionless total heat flow across the working surface that can be used as an effectiveness criterion is calculated from the formula $Q_w = \int_{\Sigma_w} q_w \, d\Sigma$. For example, values of total heat flow Q_w, thicknesses of the molten layer at the stagnation point ζ_* and exit point ζ_1, and parameter θ_* for melting rock conditions are listed in Table 1, respectively. The difference of temperature $\Delta\theta$ in the case of rock melting varies from -0.3 to $+0.3$ which corresponds to the maximum temperature variation around 330°C along the heating surface. It can be seen that the total heat flow from the working surface Q_w decreases as $\Delta\theta$ decreases. Hence the effectiveness of melting increases. In order to reduce dissipation of energy a concentration of heat near the leading edge of the working surface is required. However, the effectiveness increases slightly. On the contrary, the thickness of the molten layer is sensitive to the temperature variation. When the temperature difference $\Delta\theta$ is negative, the thickness of the molten layer at the exit point becomes small. It is undesirable, for instance, in themal drilling of rock. This is because the thickness of the molten layer along the walls of the well determines the stability of the glass like a rim that forms after the melt is solidified. The temperature difference $\Delta\theta$ along the working surface can be used as a control parameter in order to obtain the required thickness of the molten layer near the exit point ζ_1. Besides, it slightly increases the required total heat flow Q_w.

A sufficient thickness of the molten layer can also be achieved with the aid of supplementary vertical straight line segments in the generating line of the working surface. In order to determine the effective factor affecting the thickness of the molten layer, calculations were carried out for the elliptical heating surface with vertical supplementary parts of different lengths and temperature differences $\Delta\theta$. The generating curve was determined by the equation $\Phi(x, z) = 0$ where

$$\Phi(x,z) = \begin{cases} \left(\dfrac{x-x_*}{0.5}\right)^2 + \left(\dfrac{z}{1.5}\right)^2; \\ \qquad x_*-0.5 \leqslant x \leqslant x_*+0.5, \quad z \leqslant 0; \\ x-(x_*-0.5); \quad 0 \leqslant z \leqslant z_0; \\ x-(x_*+0.5); \quad 0 \leqslant z \leqslant z_0. \end{cases} \tag{30}$$

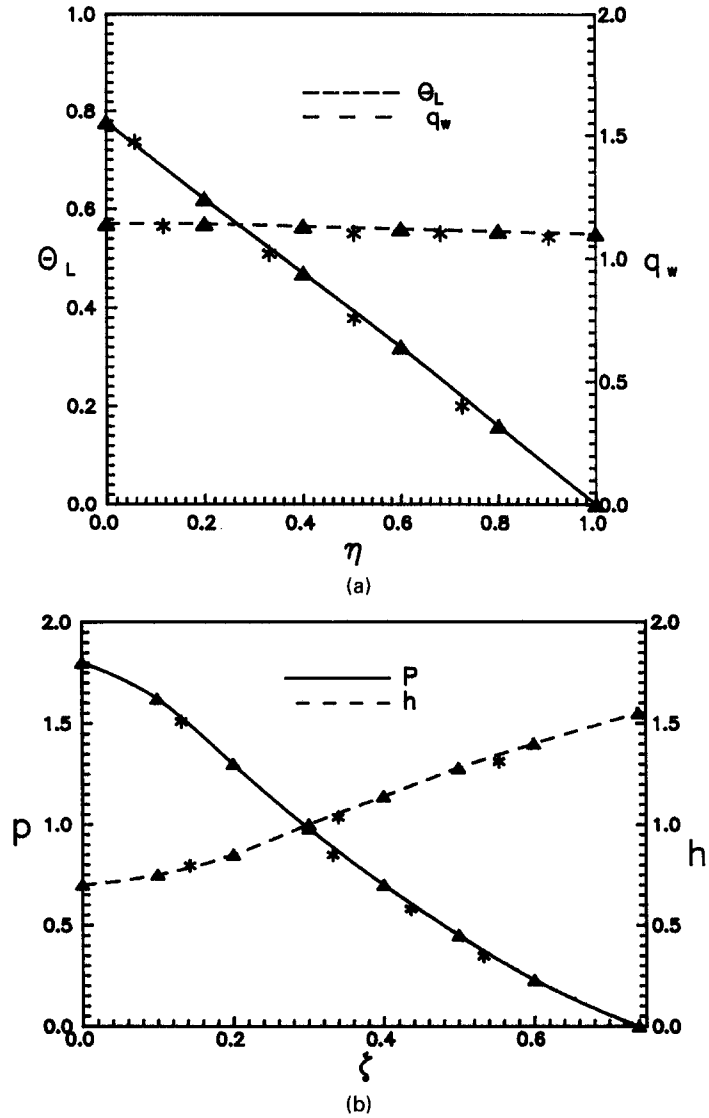

Fig. 4. Profiles of temperature and heat flux (a), and longitudinal variations of pressure and thickness (b) predicted by simplified analytical (solid and dashed lines) and numerical (* and Δ) solutions for the molten layer of ice : Δ, $\tilde{\mu} = \text{const.}$; *, $\tilde{\mu} = B_0 \exp(E/RT_1)$.

Table 1. Influence of temperature difference along the working surface of the heater on heat flow, temperature and thickness of the molten layer (rock melting by the axi-symmetric heater without central hole)

Pe	$\Delta\theta$	−0.3	−0.2	−0.1	0	0.1	0.2	0.3
6	Q_w	3.42	3.43	3.45	3.47	3.48	3.50	3.53
	θ_*	0.42	0.34	0.27	0.21	0.17	0.14	0.12
	h_*	0.3	0.24	0.19	0.15	0.12	0.1	0.08
	h_1	0.9	1.04	1.25	1.54	1.92	2.39	2.9
12	Q_w	2.49	2.50	2.52	2.53	2.56	2.58	2.61
	θ_*	0.57	0.5	0.44	0.39	0.34	0.31	0.27
	h_*	0.22	0.2	0.17	0.15	0.13	0.12	0.1
	h_1	1.11	1.23	1.37	1.54	1.73	1.95	3.18
15	Q_w	2.30	2.31	2.33	2.35	2.37	2.39	2.41
	θ_*	0.65	0.59	0.53	0.48	0.43	0.39	0.36
	h_*	0.2	0.19	0.17	0.15	0.14	0.13	0.11
	h_1	1.18	1.28	1.40	1.54	1.69	1.85	2.03

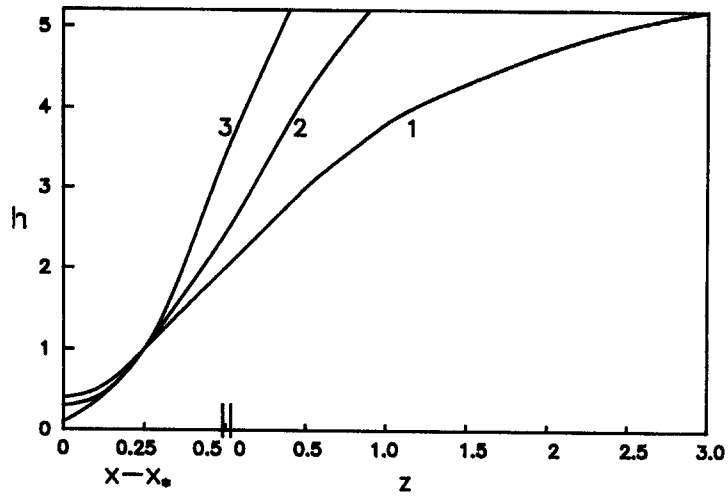

Fig. 5. Distribution of the molten rock layer thickness along the toroidal working surface of elliptical shape determined by equation (30) for $Pe = 5$. (1) $\Delta\theta = 0$, $z_0 = 3$, $Q_w = 70$; (2) $\Delta\theta = 0.1$, $z_0 = 0.9$, $Q_w = 57.6$; (3) $\Delta\theta = 0.3$, $z_0 = 0.3$, $Q_w = 52.8$.

The temperature distribution is

$$\Theta_w^1 = \begin{cases} \Theta_* + 2\Delta\Theta|x - x_*|, \\ \quad x_* - 0.5 < x < x_* + 0.5, \quad z < 0; \\ \Theta_* + \Delta\Theta + \Delta\Theta z\,; \\ \quad 0 \leqslant z \leqslant z_0, \quad x = x_* + 0.5 \\ \quad \text{or } x = x_* - 0.5. \end{cases} \tag{31}$$

The variations of thickness of the molten layer $h(\zeta)$ for different Pe, $\Delta\theta$ and z_0 are presented in Fig. 5. The results show that an appropriate layer thickness can be attained with less energy consumption by increasing the temperature difference $\Delta\theta$, rather than the vertical parts of Σ_w. An increase of $\Delta\theta$, however, has its limitations. It can induce strong overheating of the upper parts of the heater and finally cause damage. Increasing the thickness of the molten layer by elongating the vertical straight line parts of the heater does not have this shortcoming, even though it requires higher energy consumption. Therefore, an appropriate thickness of the molten layer along the walls of the bore-hole can be achieved with the aid of the corresponding temperature difference along the working surface. It should be maintained below a limit $\theta_w < \theta_{max}$ that is determined by the design of the heater. If the required thickness does not reached a further increase of the molten layer, the thickness can be obtained by elongating the working surface.

4.3. *Solution of the inverse problem in the heater*

Results of the inverse problem solution governed by equations (21)–(23) are presented in Fig. 6, where the dashed and a solid lines denote heat fluxes on Σ_w required and calculated by the equation (21), respectively. Working surface was prescribed to be of a parabolic shape generated by equation $z = P[(x - x_*)^2 + 0.25)]$. When the parameter C is found for the short heater ($P = 2$) a linear distribution

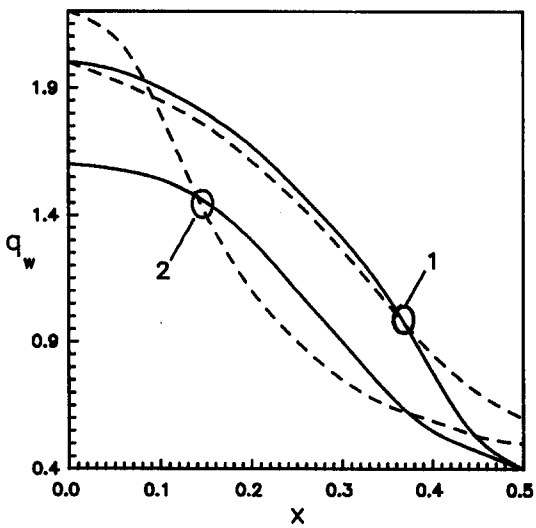

Fig. 6. Adjusted and computed (dashed and solid lines, respectively) heat flux distributions along the working surface of the heater. (1) $C = 3.75$, $p = 2$; (2) $C = 2.47$, $p = 4$.

of heat sources on the central line of the heater provides a good agreement between heat flux calculated by the equation (21) and required heat flux on the Σ_w (obtained from the solution of heat transfer problem in the molten layer). In the case of elongated heaters the linear distribution of heat sources does not provide the required heat fluxes. Therefore, more complicated multi-parametrical distributions should be chosen in order to attain better coinsideness.

5. CONCLUSIONS

(1) Heat fluxes and temperature fields in the melting solid and in the heater are determined by using a boundary elements method. The accuracy is con-

firmed by comparison with the available results for an elliptical shape of the melting surface. For an axisymmetric, ring-shaped working surface and high Peclet numbers a 2D model in Cartesian coordinates can be relevantly applied.

(2) Computed results reveal that there are two ways to control the thickness of the molten layer. One is to change the length of the heater, the other is to maintain an appropriate temperature distribution along the working surface. If the heater can not withstand high temperatures the former is preferable. Otherwise, the latter can be effectively used.

(3) Solutions of the inverse heat conduction problem in the heater show that a linear heat source in a short heater can provide a required heat flux distribution on the working surface. However, different distributions of the heat sources in the heater should be used for elongated heaters.

REFERENCES

1. M. K. Moallemi and R. Viskanta, Analysis of close-contact melting heat transfer, *Int. J. Heat Mass Transfer* **29,** 855–867 (1986).
2. B. L. Hansen, Deep core drilling in the east Antarctic ice sheet, *Proceedings of Symposium on Ice-core drilling*, pp. 29–36, University of Nebraska, Lincoln (1974).
3. V. K. Chistyakov, A. N. Salamatin, S. A. Fomin and V. A. Chugunov, *Heat and Mass Transfer in Contact Melting in Application to Thermodrilling of Glaciers*, p. 176. Kazan State University Press, Kazan (1984) [in Russian].
4. H. N. Fisher, Thermal analysis of some subterrene penetrators, *J. Heat Transfer* **98,** 485–490 (1976).
5. D. L. Lims, Melting glass-lined holes : new drilling technology, *Petrol. Engr* **7,** 80–92 (1974).
6. F. E. Moore and Y. Bayazitoglu, Melting within a spherical enclosure, *J. Heat Transfer* **104,** 19–23 (1982).
7. S. K. Roy and S. Sengupta, The process within spherical enclosures, *J. Heat Transfer* **109,** 460–462 (1987).
8. A. Saito, Y. Utaka and Y. Tokihiro, On the contact heat transfer with melting, *JSME Int. J., Ser.* 2 **31,** 58–65 (1988).
9. A. Bejan, The fundamentals of sliding contact melting and friction, *J. Heat Transfer* **111,** 13–20 (1989).
10. P. A. Tyvand and A. Bejan, The pressure melting of ice due to an embedded cylinder, *J. Heat Transfer* **114,** 532–535 (1992).
11. A. Saito, H. Hong and O. Hirokane, Heat transfer enhancement in direct contact melting process, *Int. J. Heat Mass Transfer* **35,** 295–305 (1992).
12. K. V. Taghavi, Analysis of direct contact melting under rotation, *J. Heat Transfer* **112,** 137–143 (1990).
13. M. K. Moallemi and R. Viskanta, Melting around a migrating heat source, *J. Heat Transfer* **107,** 451–458 (1985).
14. B. W. Webb, M. K. Moallemi and R. Viskanta, Experiments on melting of unfixed ice in a horizontal cylindrical capsule, *J. Heat Transfer* **109,** 454–459 (1987).
15. S. A. Fomin and P. S. Wei, The shape factor and thermal resistance in contact melting problem, *Heat Transfer* 1994, *Proceedings of the 10th International Heat Transfer Conference*, Vol. 4, pp. 25–30, Brighton, U.K. (1994).
16. H. Pinkerton and R. S. J. Sparks, Field measurements of the rheology of lava, *Nature* **276,** 383–384 (1978).
17. H. C. Carslaw and J. C. Jaeger, *Conduction of Heat in Solids*, Chap. 1, p. 510. Clarendon Press, Oxford (1959).
18. C. A. Brebbia, J. C. F. Telles and L. C. Wrobel, *Boundary Element Techniques*, p. 464. Springer, New York (1984).
19. A. N. Tikhonov and V. Ya. Arsenin, *Methods of Solution of Non-correct Problems*, p. 284. Nauka, Moscow (1979) [in Russian].
20. T. Miyazaki and W. H. Giedt, Heat transfer from an elliptical cylinder moving through an infinite plate applied to electron beam welding, *Int. J. Heat Mass Transfer* **25,** 807–814, (1982).
21. S. A. Fomin and S. M. Cheng, Optimization of the heating surface shape in the contact melting problem, *Proceedings of the Third International Conference on Inverse Design Concepts and Optimization in Engineering*, pp. 253–262, Washington, DC (1991)